Plasticity of zirconium hydrides: a coupled edge and screw discrete dislocation model

Luca Reali*[1], Mark R. Wenman[2], Adrian P. Sutton[1], and Daniel S. Balint[3]

[1] *Department of Physics, Imperial College London, UK*
[2] *Centre for Nuclear Engineering, Department of Materials, Imperial College London, UK*
[3] *Department of Mechanical Engineering, Imperial College London, UK*

Abstract

Understanding the plastic behaviour of thin zirconium hydrides is important for its implications on crack nucleation in the Zirconium alloy cladding used in fission reactors. Microvoids originate at fractured hydrides, and their coalescence may lead to the failure of the component. In this work, an innovative discrete dislocation framework is presented together with the preliminary results. The aim is to develop a model that is significantly faster than existing 3D formulations, to make it possible to run a statistical analysis on a simulated microstructure. This comes with limitations, which are discussed together with the planned developments. The model combines two planar and orthogonal simulations. In one only edge, in the other only screw dislocations are allowed, thereby describing all sides of a dislocation loop approximated as a rectangle. The two families of dislocations interact via their elastic stress, and this coupling proved to be important and significantly enhanced the dislocation density. The proposed model enables us to implement a 3D stress analysis of the hydrides. The simulations show that the most critical scenario is when neighbouring slip planes become populated with opposite-signed dislocations. This was observed both in the edge and in the screw case, and was reflected in the principal stress calculated by combining the two. It was also observed that the degree of permeability of the interface to dislocation crossing is inversely correlated to the stress inside the hydride and to the dislocation source activation.

Keywords: Coupled discrete dislocation plasticity, zirconium alloys, hydrides, computational model.

1 Introduction

Zirconium alloys are used in nuclear reactors to clad the fuel pellets. Despite having very good corrosion and mechanical resistance [1], the cladding can have problems of structural integrity due to the hydrogen coming from the water coolant, which can reach a total concentration as high as 600 weight parts per million (wppm) at the end of life of the component. Hydrogen has a low solubility limit in zirconium and forms hydrides when its concentration reaches only a few wppm at room temperature, or 400 wppm at 500 °C [2], preferentially in regions under tensile stress. Given the operating temperature of the cladding of 320-350 °C, the occurrence of hydrides is inevitable. Four different hydride phases have been reported to date: ζ-$ZrH_{0.5}$, γ-ZrH, δ-$ZrH_{1.5}$ and ε-ZrH_2. γ and δ hydrides, which have a face-centred tetragonal and cubic structure respectively, are the ones that are most commonly found in operating conditions [2]. They are crystallographically quite similar as the γ phase has cell parameters $a = 4.60$ and $c = 4.97$ nm, with a c/a ratio of 1.08, while the δ phase has a cell parameter of $a = 4.77$ nm [3], very close to the average of the two of γ. At the macroscale, hydrides appear as single precipitates up to hundred of microns in length

*Corresponding author. Email address: luca.reali16@imperial.ac.uk

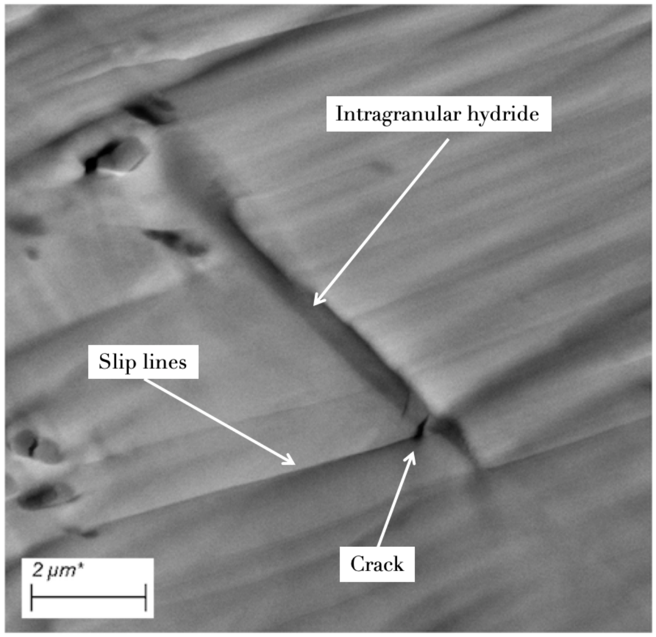

Figure 1: Intragranular micro-hydride in a Zircaloy-4 deformed until fracture. A crack can be observed near the bottom-right end (unpublished image).

(macro-hydrides), although they are actually stacks of microscopic needles up to a few microns long and tens to hundreds of nanometres thick [4, 5]. Here, with hydrides we mean the individual micro-hydride needles. Hydrides are of great concern because of a failure mechanism by the name of delayed hydride cracking [2], which involves hydrides precipitating ahead of flaws or notches and fracturing, opening a crack that can advance even at constant load by repeated precipitation and fracture cycles. However, also the hydrides present in the bulk need to be considered. In unnotched specimens, voids were found to nucleate at fractured hydrides [6] and coalesce to form a crack embryo that may lead to the failure of the material. Furthermore, the presence of hydrides has been shown to reduce the low-cycle fatigue of zirconium alloys, and the mechanism may be the same.

In the literature, zirconium hydrides are often considered much more brittle than zirconium, and this is indeed the case when referring to a macroscopic specimen [7]. However, it is the system of hydrides embedded in the parent zirconium that should be considered, and in this case the individual microscopic hydrides can show a remarkable plastic deformability. This was recognised over 45 years ago by Wanhill et al. [8], but investigated further only much later. Evidence of slip transmission from the zirconium and the hydride was reported among others by Grange et al. [6] and by Arsene and co-workers [9, 10, 11]. In titanium, which is very similar to zirconium, analogous hydrides form. A series of papers by Chen et al. [12, 13, 14, 15] clearly shows, among other results, how thin titanium hydrides can withstand more than 12000 cycles of oscillating plastic strain. Thin hydrides are severely sheared and can accommodate as much as 70% shear deformation [12]. However, as the hydrogen concentration increases, so does the hydride thickness, and cracks analogous to those found in zirconium hydrides start to appear [14]. Literature evidence on both, as reviewed by Conforto and colleagues [16], demonstrates that the hydrides are ductile if they are thinner than 400 nm, but the reason behind this ductile-brittle transition is not understood. In Fig. 1, an example of a heavily deformed intragranular hydride in Zircaloy-4 is shown.

More recently, micromechanical tests were performed on single micro-hydrides. Micropillar compression experiments showed that, in the case of $\langle a \rangle$-slip, shear bands can either cross the interface, allowing slip propagation, or stop there [17], probably leading to high localised stresses. Microcantilever bending tests on Zircaloy-4 oriented for $\langle a + c \rangle$-slip showed an increased density of geometrically necessary dislocations at the zirconium-hydride interface [18]. Microscale experiments may be crucial for a deep understanding of this phenomenon, even more so as they lend themselves to be coupled to computational works such as the one presented here.

No computational study has tried to model the plasticity within zirconium hydrides, let alone to understand the transition between thin deformable and thick brittle hydrides. Two works dealt with another important feature of zirconium hydrides. This is that, upon precipitation, they induce plasticity in the parent zirconium, due to the fact that their density is lower and therefore the phase transformation is accompanied by a volume change under the constraints imposed by the matrix [19, 20]. Tummala et al. [21] used 3D discrete dislocation dynamics to quantify the stress state in the vicinity of a single hydride, which was acting as a source of stress, and to investigate the dislocation network resulting from this stress. The goal was not to study the fracture of the hydrides, but rather to explain why they tend to precipitate stacked next to one another in a deck-of-cards fashion. Patel et al. [22] deployed 2D discrete dislocation plasticity (DDP) to rationalise the “memory effect” that is observed when hydrides undergo multiple dissolution-reprecipitation cycles. The plasticity induced by the misfit leaves behind some dislocations which generate a tensile field that is postulated to attract hydrogen in the region where the hydride used to be, facilitating a subsequent precipitation in the same place.

In this work, we use planar DDP in an innovative way. The general approach follows the conventional model by van der Giessen and Needleman [23], which features only edge dislocations, but with important differences that are explained in section 2. There has already been previous work, by Benzerga et al. [24], where three-dimensional features were incorporated into edge DDP by means of constitutive rules. However, what we do here is fundamentally different. Instead of improving an edge-only model we rather divide the problem into pure edge and pure screw, and then run the two models in the same physical space. In such a way, both the edge and the screw dislocation fields are present and, as it will be shown, interact.

To understand the plasticity of hydrides, one has to start by analysing whether the criteria for slip transmission are met. In general, this depends on the relative misorientation between neighbouring grains. There are two mechanisms to propagate plasticity from one grain to another. The first, when dislocations cross the grain boundary, is direct slip transmission. It requires a high degree of alignment between the slip systems. Alternatively, it may not be the dislocation itself which crosses the interface, but rather its elastic field. In such a way, the transmission of slip is not direct but effective, mediated by Frank-Read sources near the grain boundaries. This is known as indirect slip transmission across an interface and it occurs when several dislocations are piled up against a grain boundary. The stresses on the other side decay with the distance as an inverse square-root, as demonstrated by Eshelby et al. [25]. Locally, the stress can be very high and activate dislocation sources close to the grain boundary. Several references to experimental studies showing this phenomenon can be found in [26].

A number of different criteria were developed in the literature, as reviewed in [27], to be able to predict which slip systems will be activated in the neighbouring grain, if any, given an incoming activated slip system. The first one that was able to predict all the experiments considered in the study was the Lee-Robertson-Birnbaum criterion [28]. The three transmission rules they proposed are: (1) the alignment between incoming and outgoing slip planes should be maximised; (2) the shear stress resolved on the outgoing slip direction should be maximised; (3) because the Burgers vector is a conserved quantity [29], if the incoming and outgoing dislocations do not have the same Burgers vector, a dislocation debris with a Burgers vector equal to the difference must remain at the interface. This residual Burgers vector should be minimised. The outgoing slip plane that becomes active is determined by considering all three rules, i.e. it may not simply be the one with the best alignment or the highest resolved shear stress [28].

In the specific case of zirconium hydrides, the relative orientation of the two lattices is determined by the orientation relationship (OR) between the two phases. It is reported that, in the vast majority of cases [5, 30], both γ and δ hydrides follow the OR (illustrated in Fig. 3):

$$(111)_{\mathrm{hyd}}//(0001)_{\mathrm{Zr}}$$

$$[1\bar{1}0]_{\mathrm{hyd}}//[2\bar{1}\bar{1}0]_{\mathrm{Zr}}.$$

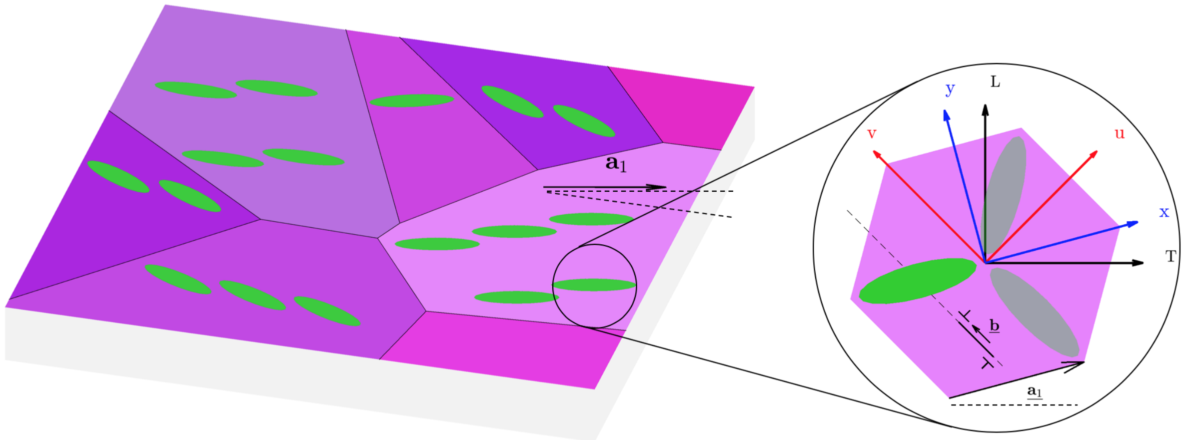

Figure 2: The texture of rolled Zircaloys is such that all the basal planes are approximately parallel to the plate surface. This affects the orientation of the micro-hydrides, one of which is being modelled in this work. In the inset, the case of a grain well oriented for single prism slip with $\boldsymbol{b}//\boldsymbol{a_2}$, in which hydrides are found aligned with $\boldsymbol{a_1}$. These assumptions make it possible to define two reference frames. One is aligned with the Burgers vector and with the edge and screw dislocation lines (uvw, in red) and one is aligned with the hydride platelet (xyz, in blue). There is an angle of $\pi/6$ separating the two. They can be at any orientation with respect to the directions defined by the manufacturing of the plate (LTN, in black).

This simply means that the close-packed planes of the cubic structure are parallel to the close-packed planes of the hexagonal parent phase, and similarly that the relative close-packed directions are also parallel to one another (in the case of zirconium, this is known as the a direction, or $\langle 2\bar{1}\bar{1}0\rangle$ using Miller indices). This result is the starting point for the setup of the DDP simulations.

2 Model formulation

The setup of the DDP model requires both the details of the texture and of the hydride distribution. Rolled Zircaloy sheets, characterised by a longitudinal (L), transverse (T) and normal (N) direction, are textured as a result of the different stresses that develop during the manufacturing [31]. The basal plane normal is orthogonal to the rolling direction [31] and contained within a cone in the N direction, whose aperture angle depends on the manufacturing route. In [6], for instance, the maximum basal pole was at $\pm$ 20° from N. To consider the configuration having the highest resolved shear stress compatible with this picture, we assume that the c direction is parallel to N and that the basal plane corresponds to the LT plane, while the orientation of the three a directions can freely rotate. This is the first assumption of the model.

In stress-free samples, macro-hydrides tend to precipitate in strings in the circumferential direction [32], whereas the micro-hydrides of which they consist are always along one of the three a directions. This means that while the former grow along the circumferential direction, their building blocks (i.e. the micro-hydrides) select the a direction which is closest to it. A schematic of this is shown in Fig. 2, and it could be applied to both γ and δ hydrides, which both grow along the $\langle 2\bar{1}\bar{1}0\rangle$ directions [33] (schematics analogue to the inset of Fig. 2 are used to describe both the γ [19] and the δ phase [34]).

Furthermore, the second assumption that we make is that the loading will act predominantly in the LT plane, which is consistent with the theory of thin shells, and that the prism slip system is the only one that is activated. This is expected in the case of room temperature deformation of non irradiated zirconium, where the critical resolved shear stress to initiate $\langle a\rangle$-basal and $\langle a+c\rangle$-pyramidal slip is about 1.3 and 3.5 higher than that for $\langle a\rangle$-prism respectively [35]. The prism slip is the easy glide system also for Zircaloy-4 at 350 °C. In irradiated conditions at 350 °C, the basal slip becomes the most favoured one, due to the presence of $\langle a\rangle$-type prismatic dislocation loops in the prism planes [36]. This would have to be

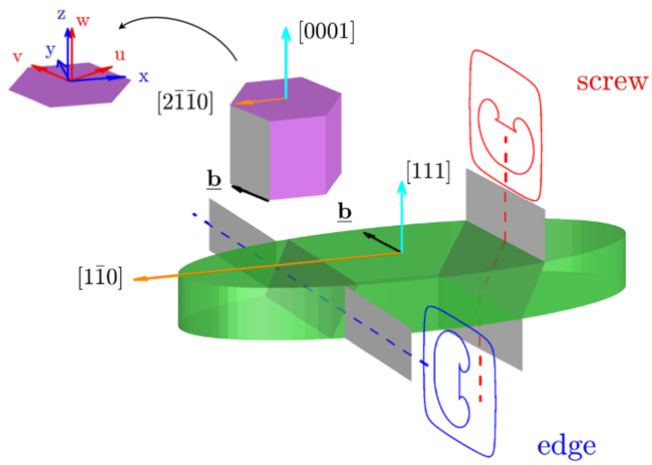

Figure 3: Micro-hydride embedded in the zirconium matrix observing the OR [2$\bar{1}\bar{1}$0]//[1$\bar{1}$0], [0001]//[111]. Only the prism slip system, highlighted in grey, is assumed to be active. Frank-Read sources are schematically shown for edge (in blue) and screw (in red) dislocations. The trajectory of the dislocation line is indicated by a dashed line. The Burgers vector does not change orientation in the two phases. The glide plane changes from prism in zirconium to close-packed {111} in the hydride by means of a rotation by 19.5°. The orientation of the reference frames used in the model, with respect to the crystallographic directions, is shown in the top left corner.

included in an expansion of the model to include the very important factor of radiation damage, together with the well known formation of defect-free channels where plasticity is localised during the deformation of irradiated metals [37, 38].

Considering now a grain that is well oriented for slip, one can see that when plasticity starts on one of the three prism planes, there will be two possible orientations for the hydrides to be sheared along their longest dimension. We focus on the one where the majority of the hydrides lie, i.e. the one closest to the circumferential direction.

Every bulk hydride is surrounded by Frank-Read sources and, depending on their relative location, will be sheared by the loops in predominantly edge or screw orientation, as shown in Fig. 3. The loops have the same Burgers vector, therefore the slip steps that they cause are the same and simply accrue.

Let us focus on one such hydride and define two coordinate systems to describe the state of stress to which it is subjected (Fig. 2, inset). The third important assumption which is made here is that the hydride is sufficiently far from the surface of the specimen to be effectively embedded in an infinite matrix. This was done for the sake of simplicity: in this way there are no boundary conditions to be satisfied, and the DDP code does not need the solution of the complementary finite element (FE) problem at every time step. Therefore, the only three sources of stress are: the external stress applied to the plate, the infinite fields of all the N_e edge and those of all the N_s screw dislocations, i.e.

$$\boldsymbol{\sigma} = \boldsymbol{\sigma}_{ext} + \sum_{N_e} \boldsymbol{\sigma}^e + \sum_{N_s} \boldsymbol{\sigma}^s, \tag{1}$$

where the external stress could have any time dependence.

The first coordinate system, namely the dislocation frame, is defined by the prism dislocation loop: u is the direction of the slip plane normal, v is the direction of the Burgers vector and of the line direction of the screw dislocations, and w is the direction of the line direction of the edge dislocations. This is the natural system to express the dislocation fields. In particular, it is useful to emphasise that, given the orientation of the dislocations, in the uvw reference frame the edge dislocations contribute to the σ_{uu}, σ_{vv}, σ_{uv} and σ_{ww} components, whereas the screw dislocations contribute to the two shear components σ_{uv} and σ_{vw}, leading to a stress tensor, in the dislocation coordinate system, of the form

$$\boldsymbol{\sigma} = \begin{bmatrix} \sigma^{ext}_{uu} + \sigma^{e}_{uu} & \sigma^{ext}_{uv} + \sigma^{e}_{uv} + \sigma^{s}_{uv} & 0 \\ \sigma^{ext}_{uv} + \sigma^{e}_{uv} + \sigma^{s}_{uv} & \sigma^{ext}_{vv} + \sigma^{e}_{vv} & \sigma^{s}_{vw} \\ 0 & \sigma^{s}_{vw} & \sigma^{ext}_{ww} + \sigma^{e}_{ww} \end{bmatrix}. \tag{2}$$

The two families of dislocations will therefore interact not only if they were to collide, but also via their elastic field. To see this, one can calculate the Peach Koehler force, $\boldsymbol{F} = (\boldsymbol{\sigma} \cdot \boldsymbol{b} \times \boldsymbol{\zeta})$, given the two line directions $\boldsymbol{\zeta}$ for edge and screw dislocations, obtaining

$$\boldsymbol{F_e} = \sigma_{vv} b\, \hat{\boldsymbol{u}} - \sigma_{uv} b\, \hat{\boldsymbol{v}} \tag{3}$$

and

$$\boldsymbol{F_s} = -\sigma_{vw} b\, \hat{\boldsymbol{u}} + \sigma_{uv} b\, \hat{\boldsymbol{w}}. \tag{4}$$

For edge dislocations, the glide force solely depends on σ_{uv}, which is the component that the two share in the stress matrix (Eq. 2), while σ_{vv} generates only a pure climb force. Also for screw dislocations in zirconium the resolved shear stress depends on σ_{uv} only, due to the fact that the trace of the prism plane is along w. In the hydride, the trace of the glide plane is at 19.5° from w (Fig. 4b). This means that the second glide component, proportional to σ_{vw}, is not very effective as it is multiplied by a factor of sin(19.5°). Moreover, σ_{vw} itself originates by other screw dislocations only, as it is assumed that the external loading has a negligible out-of-plane shear. Since the σ_{uv} component in Eq. 2 that dominates the glide of both dislocation types is the only one that is shared between the two, it is reasonable to expect a strong coupling between the two simulations. The results will show that this is indeed the case.

The second coordinate system, used for the edge simulations, is defined by the x-axis pointing along the long dimension of the hydride, which is also one of the three a directions, and by the y-axis in the normal direction in the basal plane, i.e. of the $\langle 1\bar{1}00 \rangle$ family. The two coordinate systems differ only by a $\pi/6$ rotation about the common $w = z$ direction. This is because both x, i.e. the direction of the platelet, and v, i.e the direction of the Burgers vector, need to be one of the three $\langle 2\bar{1}\bar{1}0 \rangle$ directions. These two coordinate frames may be at any angle with respect to the L and T directions of the zirconium plate, but their common axis is also the plate normal N.

The key idea in this work is that two orthogonal 2D DDP simulations can be coupled to model an inherently 3D problem, starting from a setup such as the one in Fig. 4. In the literature, there are controversial views on the morphology of the hydrides, even if δ is often described as a plate and γ as a needle [39]. As the hydride is approximated as a rectangular prism, depending on the chosen aspect ratio, both could be modelled. It can be noted that the two simulation planes are (1) orthogonal and (2) defined by a $\pi/6$ rotation between the respective coordinate systems. A choice has to be made of where to cut the simulation volume. This choice is limited as it is necessary that the simulation plane is orthogonal to the dislocation lines to fulfil the conditions for plane or antiplane strain. The fact that in a loop the pure edge and pure screw segments are orthogonal explains why the two planes are orthogonal. Under the hypothesis of prism slip, this implies that for the edge simulations the 2D cut has to be parallel to the basal plane, and for the screw simulations it has to be orthogonal to the activated prism plane. The fact that this plane is at a $\pi/3$ angle with respect to the x-axis explains the rotation of $\pi/6$ between x and u in Fig. 4 ($\pi/3$ is the angle between prism slip systems in hcp crystals). Considering now the screw geometry, this requirement means that only one of the three prism slip systems can be included. Thus, in order to maintain the symmetry between the edge and the screw models, which represent parts of the same three-dimensional prism loops, single slip conditions were enforced in all the simulations.

2.1 The DDP formulation

The proposed computational approach is similar in many aspects to conventional planar DDP [23], but with two important differences: the absence of the FE correction and the fact that we do not consider

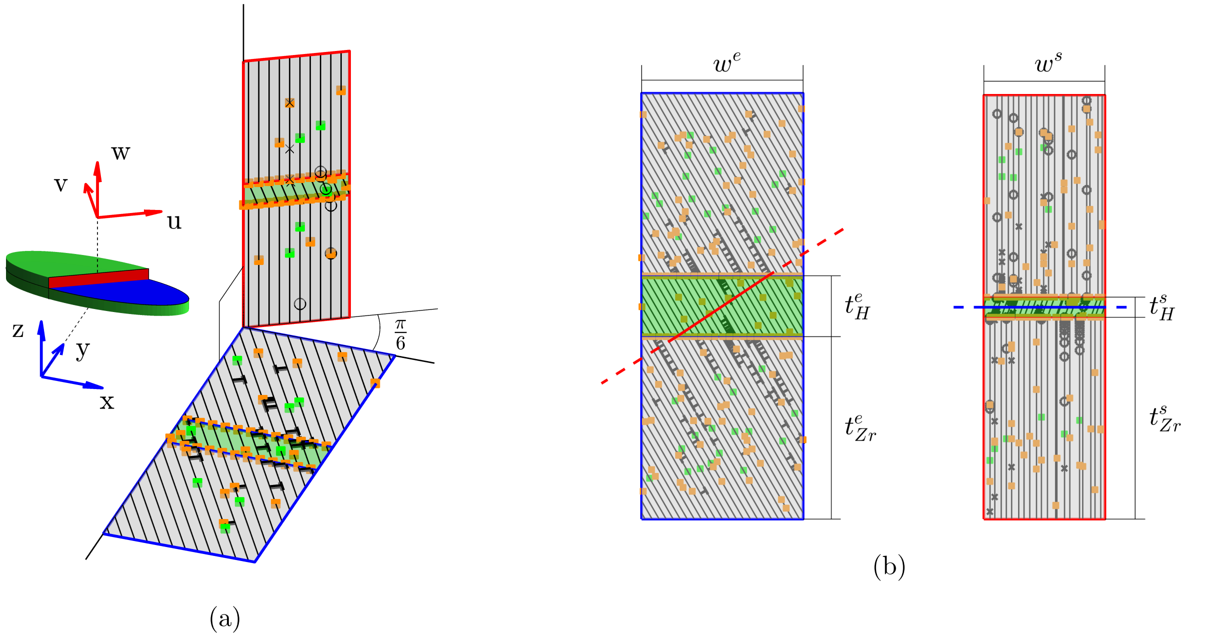

Figure 4: (a) Schematic in 3D of the two planar simulations with respect to the hydride. The section of the edge simulation (xy plane, in blue) is parallel to the basal plane, on which the platelet lies. The screw simulation plane (uw, in red) cuts the hydride through the thickness in the direction orthogonal to the basal plane. The two simulation planes are orthogonal and the normal of the screw section is parallel to the slip planes of the edge simulation. Point sources (in green) and obstacles (in orange) are randomly distributed across the slip planes. (b) The two simulation planes, each showing the trace the other. Edge dislocations are represented with a T-shaped symbol, positive screw with circles, negative with crosses. The prism planes where slip takes place, whose traces are drawn in both simulation planes, are all parallel to the vw plane.

only edge dislocations but also screw dislocations. Except for the coupling mediated by the elastic stress field, the two simulations run independently. The relevant numerical parameters are reported in Tab. 1. Zirconium and its hydrides have similar elastic properties, with e.g. a less than 5% difference in the Young's modulus [40]. For this work, the elastic moduli were assumed to be the same. Similarly, the change in length of the Burgers vector (0.6% in the case of γ hydrides) is negligible. The fact that the values of the elastic constants and Burgers vector are very similar for the two phases is of crucial importance, as it enables us to make use of the simple expressions for a dislocation in an infinite medium, regardless of it being in the zirconium or in the hydride.

For the edge simulations, the slip plane spacing is constant and fixed to $100b$, the value that was first used by van der Giessen and Needleman [23] and is now established in the literature as sufficiently small to resolve slip localisation. For the screw simulations, the spacing is variable and randomised using a Gaussian distribution so that the average spacing does not exceed $100b$. This ensures that the planes in the two simulations do not correspond to the same crystallographic one, and that one dislocation in one simulation can never cross another dislocation in the other. In fact, the opposite would be very unlikely. Crystallographically, prism planes have a spacing of $\sqrt{3}\,b/2$, but in DDP about one in 115 is modelled. In reality, Frank-Read sources could be present in any of the planes. Therefore, the likelihood that one edge and one screw source are on the very same plane, if they are randomly assigned to two crystallographic planes in the same interval of width $100b$, is 1 in 115.

A pinned dislocation segment can generate a full loop by means of the Frank-Read mechanism. To emulate this in standard DDP [23], one assumes that the segment is perpendicular to the simulation plane and of pure edge character, hence a point in the 2D section. Two dislocations are injected into the simulation when the critical resolved shear stress exceeds a critical value τ_{nuc} for a time $t > t_{nuc}$. In this work, the same representation is used for the edge simulation, and similarly in the screw simulations,

Table 1: Numerical parameters unless stated otherwise (e: edge, s: screw, Zr: zirconium, Hyd: hydride). Sources and obstacles strengths follow a Gaussian distribution whose mean value is reported and whose standard deviation is 10%.

Material	μ	b	ν	B	
	[GPa]	[nm]	[-]	[Pa·s]	
	33	3.23	0.3	e: $5 \cdot 10^{-5}$ s: 10^{-4}	
Sources	ρ_{src}	L_{nuc}	τ_{nuc}	t_{nuc}	
	[µm^{-2}]	[b]	[MPa]	[ns]	
Zr:	10	500	65	2.5	
Hyd:	0/20	250	116		
Obstacles	ρ_{obs}	τ_{obs}		τ_{obs}^{int}	
	[µm^{-2}]	[MPa]		[MPa]	
Zr:	50	325		325/3250/∞	
Hyd:	100				
Comput./ Loading	v_{cut}	δt	t_{end}	σ_0	$\dot{\sigma}$
	[m/s]	[ns]	[µs]	[MPa]	[MPa/µs]
	1000	$5 \cdot 10^{-2}$	2/4	100	50/25
Geometry		t_{Zr}	t_H	w	
		[µm]	[µm]	[µm]	
	e:	0.97	0.32	0.86	
	s:	1.0	0.2	0.6	

except for the fact that the pinned segment is of pure screw character. It is assumed that the two simulation planes cut only pinned segments of the same kind. In reality, it does not matter what is the nature of the pinned segment, but rather that of the part of the loop impinging on the hydride. Since the Burgers vector is always the same, this manner of source representation can be done without loss of information.

To determine the source activation stress we follow the analysis by Foreman [41] and consider

$$\tau_{nuc} = A\,\frac{\mu b}{2\pi L_{nuc}}\left[\log\left(\frac{L_{nuc}}{r_0}\right)\right], \tag{5}$$

where μ is the shear modulus and r_0 is the core radius. A is a constant that takes the value of 1 and $1/(1-\nu)$ for a pinned segment having edge and screw character respectively (ν is the Poisson's ratio). The dependence on the core radius is weak, and in the model it was considered that $r_0 \sim b$.

The only input parameter of the model is the pinned segment length L_{nuc}, which is assumed to follow a Gaussian distribution. The dipole is introduced with a spacing $2L_{nuc}$. Opposite-signed dislocations annihilate one another if they come closer than the annihilation distance of $8b$ [23].

At every time step δt, the velocity of each dislocation is calculated and then used to update its position. DDP usually implements a linear relationship $v_i(s) = F_i(s)/B$ between the velocity of the i-th dislocation and the Peach-Koehler force, where the scaling factor B is the drag coefficient and s is the coordinate of the dislocation on its slip plane. The drag coefficient of edge dislocations ($5 \cdot 10^{-5}$ Pa·s) was set to half of that of screw dislocations (10^{-4} Pa·s), using approximately the same ratio between the two as in [21].

Chakravarthy et al. [42] proposed a slightly different expression for the velocity, obtained by linearisation of the backward Euler integration. In our model, we adapt their result and calculate the velocity as

$$v(s) = \frac{F(s)}{B\left[1 + \left|\frac{1}{B}\frac{\partial F}{\partial s}\delta t\right|\right]}, \tag{6}$$

where $\partial F/\partial s$ is the directional derivative of $F(x,y)$ along s. If θ is the angle between the slip plane and the x-axis, it evaluates to $\frac{\partial F}{\partial x}\cos\theta + \frac{\partial F}{\partial y}\sin\theta$. The analytic expressions of the stress components and their derivatives that are required in Eq. 6 are included in App. A. When the standard forward Euler method is used, dislocations in pile-ups tend to vibrate back and forth unless the time step is kept very small. In the case of a pile-up, a dislocation is being forced by the applied stress against others that repel it, therefore it feels a gradient in the opposite direction that, scaling with the inverse of the square of the separation between them, becomes very large as they come sufficiently close. In [42], at the denominator there is a minus sign and no absolute value. One can see that such a correction introduces a damping that deals with this issue. We observed that, by including this correction, the smallest time step not leading to dislocations vibrating in an isolated single pile-up could be increased by about two orders of magnitude. However, when opposite-signed dislocations are about to collide, and must be annihilated, this functional form implies first an acceleration caused by the gradient, and possibly an unphysical reversal of the sign of the velocity when they come sufficiently close that $\frac{1}{B}\frac{\partial F}{\partial s}\delta t > 1$. Observations of opposite-signed dislocations bouncing off each other led us to implement Eq. 6 instead.

Dislocations are stopped at obstacles, which are characterised by a strength τ_{obs} that is drawn from a Gaussian distribution, and unpinned if the resolved shear stress acting on them exceeds τ_{obs}. Obstacles can be of two kinds. Internal obstacles are randomly distributed along the slip planes, and they represent the forest hardening caused e.g. by dislocations lying on other planes and not explicitly modelled. Zirconium alloys exhibit low strain rate sensitivity similar to other hcp alloys, e.g. in the 10^{-5}-10^{-2} s^{-1} range [43, 44]. Some mechanisms of high strain rate sensitivity are captured naturally in DDP via the source nucleation time and drag coefficient. Low strain rate sensitivity can also be captured in DDP by introducing thermally activated escape of dislocations from obstacles - this has been shown to be the source of low strain rate sensitivity in titanium alloys [45]. However, as rate sensitivity is a secondary aspect of the dislocation transmission processes studied here, a single loading rate was used in all simulations and additional sources of rate sensitivity were not considered. An obstacle of another kind is the grain boundary, which in this case is the hydride interface. Even if the Burgers vector need not change upon crossing the interface, the slip plane has to rotate about it by 19.5°, which is the angle between the prism planes and the $\{111\}$ planes. In the case of edge dislocations, this requires core diffusion [29], while in the case of screw dislocations it involves cross-slip [46]. Both mechanisms, which are thermally activated, hinder the slip transmission. Obstacles are placed at the interface to capture this. The strength of the two types of grain boundary transmission barriers would naturally differ, however they were taken to be the same for simplicity. All simulations in this work are carried out at constant temperature, thus it is sufficient to have a constant interfacial obstacle strength τ_{obs}^{int}. If the temperature were also to be a variable, a more detailed treatment of the slip transmission would be required. All the point sources and the other obstacles are randomly distributed with densities ρ_{src} and ρ_{obs} respectively.

Both the motion of the dislocations and their nucleation is controlled by the total stress. If the two simulations were considered individually, the total stress would be the sum of the external stress and that coming from the dislocations in that simulation. When the two simulations are coupled, before calculating the resolved shear stress on dislocations and on sources of, say, edge character, a separate function calculates the stress that is coming from the screw dislocations, and vice versa.

The boundaries of the simulation cell are transparent and dislocations can freely exit. As the load increases monotonically, dislocations that have exited the simulation cell will continue to drift apart to infinity. Hence, their influence on the centre of the cell where the hydride is located will be fleeting as well. These dislocations are removed from the simulation for computational efficiency. If the load were to reverse its sign, e.g. in the case of cyclic loading, this approach would no longer be acceptable. Another possibility for dealing with this situation, not explored in this work, is to implement periodic boundary conditions (PBCs). The reason for not implementing PBCs, in this particular case, is that hydrides precipitate either isolated or in a stacked deck-of-cards fashion (while PBCs would give a doubly-periodic structure that is not represent the actual hydride pattern observed in the material). The code was written in Matlab, using subroutines written in C++ to calculate the stress components and their gradients.

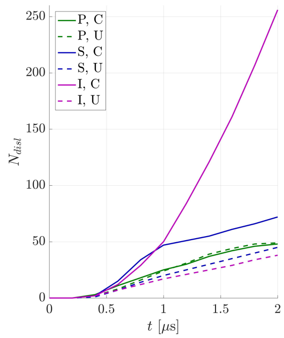

(a) Edge dislocations.

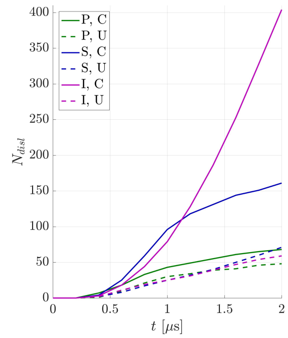

(b) Screw dislocations.

Figure 5: The time evolution of the number of (a) edge and (b) screw dislocations in simulations with source-free hydrides follow the same trend. Solid lines show simulations where edge and screw dislocations are coupled (C), as opposed to the uncoupled (U) case shown by the broken lines, for permeable (P), semi-permeable (S) and impermeable (I) interfaces. In the latter case the coupling stress causes a self-amplifying mechanism that quickly leads to a very high dislocation density.

3 Results

Two sets of simulations were performed. First, we investigated the influence of different interface permeabilities, in the case of a source-free hydride, focusing on the evolution of the number of dislocations (Figs. 5 and 7 and Tab. 2). This was done to show the importance of the coupling stress, which we define as the shear stress that the edge dislocations exert on the screw simulation, and vice versa. These two stresses are determined by evaluating σ_{uv}^{e} and σ_{uv}^{s} at the location of the screw and edge simulation plane respectively. Each random population of sources and obstacles was used to run two simulations, identical except for the coupling stress which was included (coupled, C) or not included (uncoupled, U). As the total number of sources and their locations are the same, any difference on the generation of dislocations is due to the coupling stress. In a second set, sources in the hydride were included and the stress inside of it was calculated, again for different interface permeabilities (Figs. 8 and 9 and Tab. 3). In both cases, results are averaged over ten simulations. The material was subjected to a stress $\boldsymbol{\sigma}_{ext} = \boldsymbol{\sigma}_0 + \dot{\boldsymbol{\sigma}}t$ resulting from a uniaxial tension of magnitude $\sigma_0 + \dot{\sigma}t$ applied in the basal plane and at 45° from the single slip system, i.e. 15° from the y-axis. In the first set σ_0=100 MPa, $\dot{\sigma}$=50 MPa/µs and the total simulation time was t_{end}=2 µs. In the second set σ_0=100 MPa, $\dot{\sigma}$=25 MPa/µs and t_{end}=4 µs.

Considering both edge and screw dislocations, in two orthogonal planar frameworks, has two consequences. First, they elastically interact with each other. Second, a 3D stress analysis is possible, despite the planarity of the individual simulations. This interaction is mediated by the coupling stress. First, it was determined whether the coupling factor was indeed important, or if it could be neglected for the sake of efficiency. To do so, a first group of simulations was set up so as to maximise the coupling effect, exploiting the long-ranged pile-up stresses. This was achieved by preventing direct slip transmission across the interface, and by having a source-free hydride. In such a way, the plane of one simulation is sandwiched between opposite-signed pile-ups from the other simulation, with an expected enhancement of the external stress. This makes use of the fact that the sources naturally generate dipoles of the correct sign so that the stress ahead of the pile-ups that they originate has the same sign as the external one. Such a setup is not lacking a physical grounding, at least as an extreme case: Tummala et al. [21] considered the case of a hydride that was inducing plasticity in its surroundings, but did not contain any source or obstacle inside it. It is also somewhat similar to what Benzerga et al. [47] did in an early study on second phase particles in aluminium alloys, where they considered the case of a source-free intermetallic wall between the two sides of the matrix. Moreover, micromechanical tests [17, 18] show that slip bands in some cases do stop at the interface, creating a situation close to that of these simulations.

Table 2: Effect of the coupling stress on the mean and standard deviation of the number of dislocations in coupled (N_{cp}) and uncoupled (N_{uncp}) simulations. In the impermeable case (I), all the pile-ups enhance the external stress. This results in a very large increase of the dislocation density. In the permeable (P) and semi-permeable (S) cases, the coupling stress could act so as to either enhance or decrease the external stress.

	Type	N_{cp}	N_{uncp}	N_{cp}/N_{uncp}
P	edge	48±15	49±14	0.98
	screw	68±32	48±20	1.42
S	edge	72±20	45±10	1.60
	screw	161±30	71±27	2.27
I	edge	256±144	38±9	6.74
	screw	404±200	59±16	6.85

The impermeable (I) case was then compared against the case of a permeable interface (P), where the interfacial obstacles have the same strength as the internal obstacles, and a semi-permeable interface (S), where $\tau_{obs}^{int} = 10\ \tau_{obs}$. Using this setup, the averaged results over ten simulations showed a significant enhancement in the number of dislocations when the respective coupling stresses were included in the planar edge and screw simulations. Fig. 5 shows the time evolution of the number of edge and screw dislocations, in the three aforementioned cases, for coupled and uncoupled simulations. The first thing to note is that coupling the simulations has a significant effect, especially on the number of screw dislocations. This is clearly visible in the last column of Tab. 2, which reports the number of dislocations at the end of the simulation. Second, the extent to which the coupling stress was significant was very large in the impermeable case, and decreased for the semi-permeable and especially for the permeable cases. This was expected and can be rationalised by thinking about the pile-up stresses. Pile-ups originate a strong, localised stress in front of them and a (slightly) less strong stress, of the opposite sign, behind the last of the dislocations of which they are composed of. By having a source-free hydride and impermeable interfaces, all the pile-ups induce a coupling stress on the other simulation that is of the same sign. As soon as the zirconium-hydride interface allows the transmission of dislocations, a pile-up will form on the other (hydride-zirconium) interface, and exert a coupling stress of the opposite sign. Third, and most importantly, contrary to the P and S cases, which show a tendency to reach a saturation in the dislocation density, in the I case a very rapid and divergent growth in the number of dislocations was observed. This was due to a self-amplifying positive feedback effect whereby growing edge dislocation pile-ups cause screw dislocation sources to remain active, and vice versa. What is normally observed in DDP is that a source that causes a pile-up will cease to nucleate dipoles as soon as the back stress from the pile-up becomes large enough. For example, if the coupling stress caused by edge dislocation pile-ups is strong enough, it will compact the screw dislocation pile-ups. As a consequence, they are pushed away from their sources,

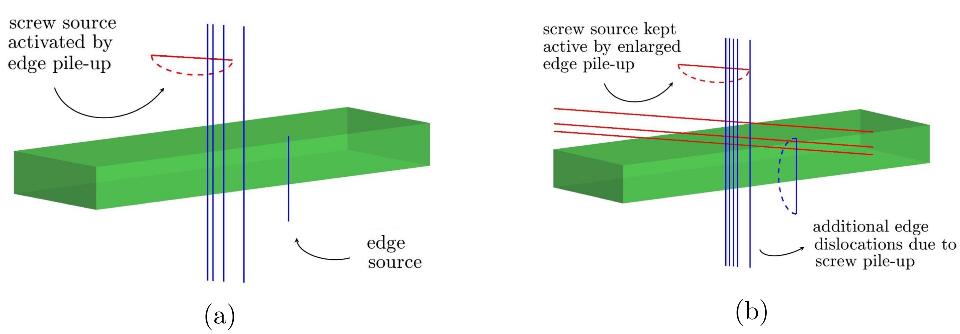

Figure 6: Schematic illustrating the positive feedback loop leading to the marked increase in N_{disl} as the permeability of the interface is reduced. (a) A pile-ups of one kind, say edge (in blue), activates a screw source. (b) This produces a screw pile-up (in red) that increases the stress acting on the edge source.

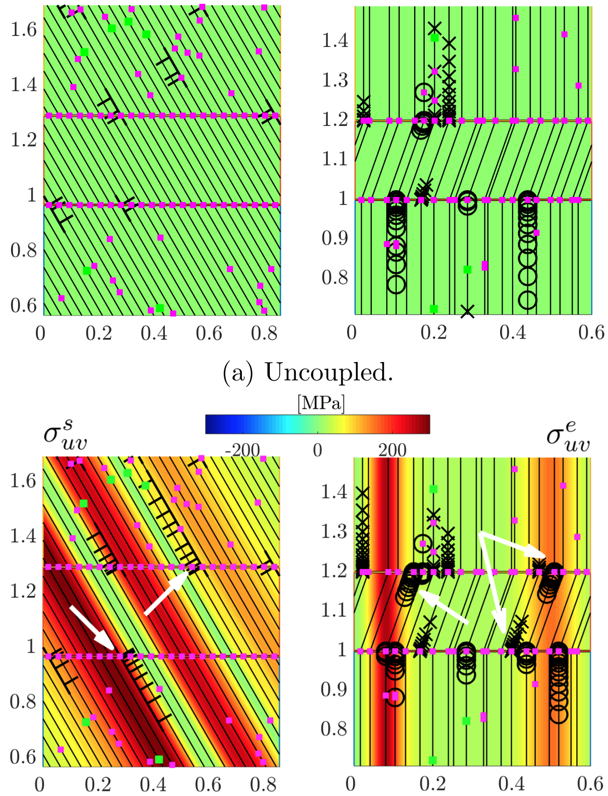

(a) Uncoupled.

(b) Coupled.

Figure 7: The effect of the coupling stress in the semi-permeable case for a source-free hydride. The dislocations are plotted on a map of the two coupling stresses σ_{uv}^{s} and σ_{uv}^{e}. White arrows highlight examples of pile-ups or slip transmission that would either not be there, or be less developed, were the coupling to be ignored. Axes in µm.

which diminishes the back stress on the sources, hence enhancing their activation. This in turn has the consequence of increasing the coupling stress on the edge dislocation sources, completing the feedback loop. With impermeable interfaces there is no limit to the number of dislocations in the pile-ups and, consequently, to their stress. The self-amplifying increase in the source activity is schematically illustrated in Fig. 6. If the permeability of the interface is increased, as expected, the effect of this enhancement mechanism is greatly reduced (Tab. 2).

The cross interaction between the simulations is best visualised by superimposing the stress caused by one kind of dislocation on a plot showing the positions of the other. This is done in Fig. 7. It is clearly possible to associate regions of high coupling stress with the onset of new pile-ups or the magnification of existing ones, with associated consequences for the overall stress state of the hydride.

Using the data in Tab. 2, the dislocation density was estimated to be about 0.3-1.4$\times10^{14}$ and 0.5-3.0$\times10^{14}$ m^{-2} for the edge and screw dislocation simulations respectively, totalling to about 1-4$\times10^{14}$ m^{-2}, a value that is, as expected, slightly higher than what is measured in hot-rolled and annealed Zircaloy-4 samples [48, 49].

A second set of simulations included the presence of sources in the hydride, with the aim of quantifying the stress state inside the hydride. Here, we considered the same P and S cases, but not the impermeable interface due to the unrealistically high stresses and divergence in the number of dislocations that posed a limit on the maximum simulation time. The coupling stress is always included. We believe that the effect of the sources in the hydride may be important. First, one can imagine how the effect of the pile-up stresses may be even greater for hydride sources. The way the coupling stress is calculated relies on the fact that the dislocations remain straight and do not bend around the hydride, which is something that we need to assume because of the planar nature of the simulations. But even if they were able to bend,

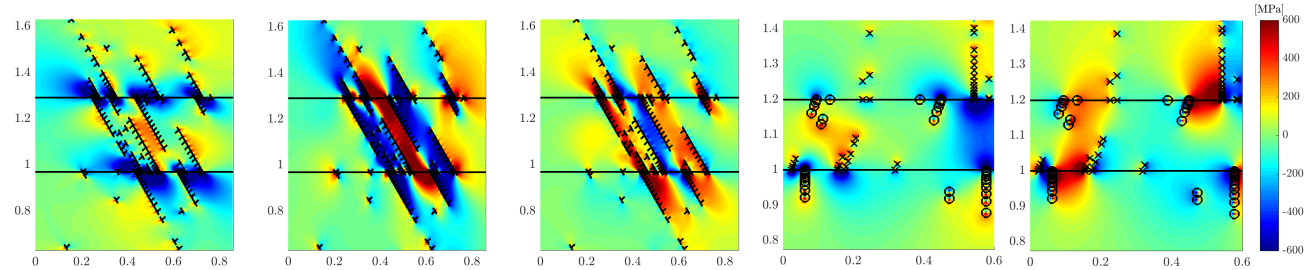

(a) σ_{xx} (b) σ_{yy} (c) σ_{xy} (d) σ_{uv} (e) σ_{vw}

Figure 8: Contour plots of one of the simulations with semi-permeable interface: three stress components from the edge simulations (a-c) in the xyz frame and two components from the screw simulations (d-e) in the uvw frame, which feed into the 3D stress analysis. It is convenient to use two different coordinate systems due to the setup of the analysis, as explained in Fig. 4. Axes in µm.

they would still exert a similar stress inside the hydride to that predicted here. Second, there is evidence that the dislocation density is about one order of magnitude higher in the hydride than in the matrix [50, 48]. This has two consequences. The source density can be expected to be higher, and the average pinned length shorter, leading to a higher activation stress according to Eq. 5. This means more potential nucleation events, but requiring a higher stress. We assumed a factor of two more and less, respectively, for ρ_{src} and L_{nuc} inside the hydride.

The results in Tab. 3 show a much stronger tendency for nucleation internal to the hydride in the semi-permeable case, with almost an 8-fold and a 4-fold increase in the edge and screw simulations respectively. Each hydride source generated, on average, about 2 edge dipoles and 6 screw dipoles if the interface was permeable, and about 15 edge and 24 screw dipoles if it was semi-permeable. This amplification is a result of having more numerous pile-ups both inside the, say, edge simulation, and in the other one (the latter effect being mediated by the coupling stress).

3.1 The stress analysis

The purpose of using DDP in this project is to quantify the stress state inside and in the surroundings of the hydride and, in the future, to quantify the likelihood of fracture. The outcome of the coupled edge and screw simulations is given by three and two stress components respectively, an example of which is depicted in Fig. 8. The stress field of a dislocation is singular as it scales with the inverse square of the distance from the core, and was here regularised by introducing a constant $4b^2$ in the denominator. These components are used to calculate the simplest indicator that can be used for assessing crack nucleation, if one assumes a Mode I opening, which is the first principal stress σ_I obtained by diagonalising the stress tensor.

Using conventional DDP a principal stress map can be calculated, such as the one presented in Fig. 9a, which only features information from the edge dislocations. Using only the screw dislocations, on the other hand, gives a map such as the one in Fig. 9b. The values of the peak stress thus obtained are summarised in the first two columns of Tab. 3, averaged over the ten simulations performed for the edge and screw cases. The stress was calculated on a grid whose size was set to 0.001 µm after a convergence analysis.

To decrease the computation time, the dislocations that exit the simulation cell are removed from the simulation. This will have an effect as their back stress on the sources near the boundaries will be removed as well. As the quantity of interest is the stress inside the hydride, the effect of this simplification has to be investigated. The simulations summarised in Tab. 3 were repeated, this time without removing the dislocations and instead letting them glide to infinity. The average change in the maximum stress was found to be 3.0% when only edge dislocations are considered, 6.7% for only screw dislocations and 4.0%

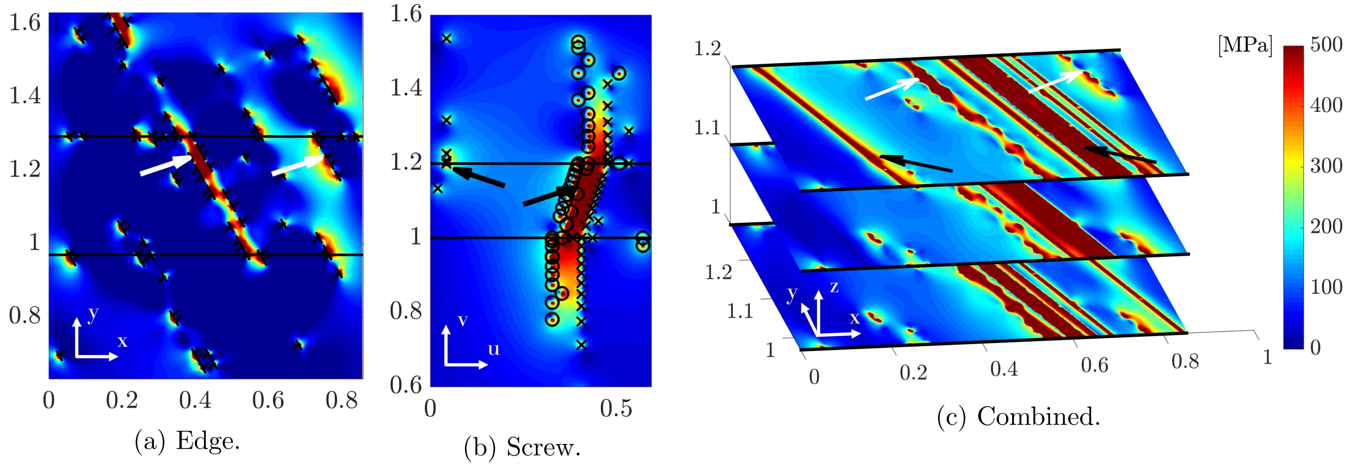

Figure 9: σ_I can be calculated from either of the planar simulations. In (a) only the edge dislocations enter the diagonalisation and in (b) only the screw dislocations. However, a more accurate state of stress is given by the superposition of the two. This is shown in (c) for the approximately 0.9×0.3×0.2 µm hydride. The slice plot shows cuts parallel to the edge simulation, which depending on their z coordinate are affected by the screw simulations. It is possible to identify regions of high stress attributable to the edge and screw dislocations, as highlighted by the white and black arrows respectively. The two simulations give rise to stresses of comparable magnitude. The axes (units of µm) are shown in white. Black lines mark the Zr-hydride interface in (c).

for edge and screw combined. This should be compared with the significant increase in the simulation time, which on average went from about 8 to 22 minutes in the P case, and from about 9 to 23 minutes in the S case. Thus, with an error of order 5%, the simulation can run about 2.5-3 times faster. The calculations were carried out on a workstation equipped with a quad-core 3.40 GHz processor and 16 GB of RAM.

One interesting observation on the stress building up inside the hydride can already be made: by analysing several simulations, it appears that there are two distinct situations of stress intensification. The first is, unsurprisingly, caused by dislocation pile-ups such as the ones indicated by the rightmost arrow in Fig. 9a or by the leftmost arrow in Fig. 9b. They can locally reach high stress values, but also decay fairly rapidly if considering lengths of the order of micrometres. The second arises when two neighbouring slip planes become significantly populated with opposite-signed dislocations (for edge dislocations, in addition to this requirement, the two missing half-planes must be facing each other). In this case, a channel of high tensile (for edge) and shear (for screw dislocations) stress develops. This can be potentially much wider, as it scales with the slip band spacing ($\sim 100b$) and with the hydride thickness ($\sim 10^2$ nm).

The additional advantage of combining edge and screw simulations is that the stress analysis becomes three-dimensional, as clearly the two stress fields superimpose. The two components σ_{uv} and σ_{vw} from the screw simulations were rotated so as to express all the stresses in the xyz coordinate system, and the resulting stress matrix has 6 non-zero components. The maximum values of σ_I are reported in the third column of Tab. 3. It is interesting to note that the maximum stress of the two simulations combined is approximately equal to the square root of the sum of the squares of the two planar simulations.

4 Conclusions and future developments

In this paper we present a new 2.5 DDP method, which entails running two planar simulations at the same time, pure edge and pure screw, which are coupled by their elastic interaction. The application is to the plasticity of thin zirconium hydrides. The first objective was to develop a very fast code, faster than conventional edge DDP, but one which also captures the essential 3D nature of the problem. This

Table 3: Mean value and standard deviation of σ_I^{MAX} reached inside the hydride, calculated using only edge (e), only screw (s), or combining both types of dislocations (c), and number of dipoles (N_{dip}) nucleated by sources inside the hydride at the end of the simulation. A semi-permeable interface (S), as opposed to a permeable one (P), leads to significantly higher stresses and internal source activation.

	σ_I^{MAX} [GPa]			N_{dip}	
	e	s	c	e	s
P	2.45±0.09	1.49±0.10	2.79±0.42	12	19
S	3.26±0.01	3.45±0.71	4.26±0.77	91	73

will make it possible in the future to run a large number of simulations to explore the statistics of e.g. probability of fracture given the hydride geometry and/or their number density. The simulations led to the following observations:

1. The coupling between edge and screw dislocations, via their common shear component, is significant. In the case of impermeable interfaces, it led to a more than 6-fold increase in the number of both types of dislocations. This effect was reduced for permeable or semi-permeable interfaces, but remained important nonetheless.

2. A stress analysis was carried out on the two planar simulations, both individually and jointly. First principal stress maps showed that the most critical situation arises when neighbouring planes happen to have a high slip activity of opposite-signed dislocations.

3. The combined stress analysis, where high stresses due to edge and screw dislocation channels superimpose, showed values higher than those attained by the two individually. On average, an increase of 14% (permeable case) and of 31% (semi-permeable case) was observed with respect to only edge dislocations, and 87% (permeable case) and 23% (semi-permeable case) with respect to only screw dislocations.

This model makes use of justified simplifications, which we summarise here together with possible developments that are already underway. In most cases, the assumptions can be removed but at the expense of computation time.

- Edge and screw simulations have only one active prism slip system. This is reasonable for those grains having one of the three prism planes well oriented for slip. The edge simulations could include them all, but in the screw simulations the antiplane strain requirement allows only one to be modelled at a time. As the model stands, this could be mitigated by including an adaptive density of obstacles, which however would add one more unknown parameter.

- One single hydride is modelled here. In reality, hydrides tend to precipitate as macro-hydrides in a "staircase" stack. If these building blocks are sufficiently spaced apart, every single micro-hydride will be predominantly affected by its two nearest neighbours, especially for the dislocations that are generated in their surroundings due to the volume misfit [21, 22]. This means that a stack of just three hydrides should be sufficient to appropriately model the middle one.

- In the current formulation, we assume that the matrix is infinite. There are no boundary conditions but only an external stress. This means that the model is fully analytical and there is no FE correction problem. Including the FE correction would enable a direct comparison with micromechanical tests, which may be very interesting given the data that has recently become available [17, 18].

- The interface was modelled in a very simplistic way, with only a layer of obstacles of unknown strength. In reality, both an elastic field caused by the volume misfit, and interfacial dislocations may be present. This is not easy to include as there is no experimental characterisation available of the local stresses, and there is no consensus on the nature of the interfacial dislocations, if present. Early studies report the presence of $\langle a \rangle$-type dislocations [19], but they may have been an artefact of the sample preparation [51]. Similar $\langle a \rangle$-type dislocations were also reported more recently [52], but they were not present in another paper, in which $\langle c \rangle$-type dislocations were observed instead. The stress field could be approximated by a misfitting inclusion [53], but the relative long-range stress would be zeroed by the presence of the dislocations typical of semi-coherent interfaces [26]. Finally, interfacial $\langle a \rangle$-type dislocations could also react with the glide prism dislocations. It is presumed that the misfit stresses may have an impact on the results. A study on the different effect of all these variables is under development.

- The hydrides considered in this work are intragranular, i.e. the matrix on either side has the same crystalline orientation. Hydrides are also found at the grain boundaries. For these intergranular hydrides, the orientation relationship can in general be observed only on one of the two sides. Hence, the Burgers vectors considered in this work can be aligned only on one of the two interfaces. Hence, the slip propagation is expected to be harder, with more pronounced pile-ups developing at least on one of the two interfaces. This can be incorporated into the present framework by making the interfacial obstacle strength dependent on the misalignment, and by using the law of conservation of the Burgers vector to deal with the associated Burgers vector debris.

Acknowledgements

This work was supported through a studentship in the Centre for Doctoral Training on Theory and Simulation of Materials at Imperial College London funded by the EPSRC (EP/L015579/1) and through an industrial collaboration with Rolls-Royce plc.

Data availability

The data that support the findings of this study are available on request from the corresponding author (L.R.). The data and the code are not publicly available due to them containing information that is commercially sensitive or not in the interest of commercial/national security."

A Dislocation stresses and gradients

A.1 The screw dislocation

Let us consider a screw dislocation having the Burgers vector along z, i.e. $\boldsymbol{b} = (0, 0, b)$. The magnitude of the glide component of the Peach-Koehler force is given by

$$F(x, y) = \hat{\boldsymbol{n}}\boldsymbol{\sigma}(x, y)\boldsymbol{b} = -b \sin\theta \sigma_{xz}(x, y) + b \cos\theta \sigma_{yz}(x, y). \tag{A.1}$$

We note that only the stress tensor here depends on the position. As s is a coordinate along a straight line, $\frac{\partial F}{\partial s} = \cos\theta \frac{\partial F}{\partial x} + \sin\theta \frac{\partial F}{\partial y}$ leading to

$$\frac{\partial F}{\partial s} = -b \cos\theta \sin\theta \frac{\partial \sigma_{xz}}{\partial x} + b \cos^2\theta \frac{\partial \sigma_{yz}}{\partial x} - b \sin^2\theta \frac{\partial \sigma_{xz}}{\partial y} + b \sin\theta \cos\theta \frac{\partial \sigma_{yz}}{\partial y}.$$

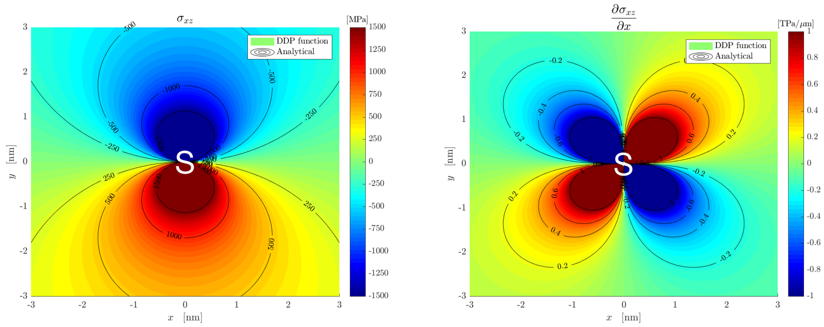

(a) (b)

Figure A.1: Plots of the (a) σ_{xz} components, and (b) of its partial derivative with respect to x, of an isolated screw dislocation at the origin.

The total stress acting on each dislocation is given by the sum of the external stress and the stress field of each of the N dislocations $\boldsymbol{\sigma}_s$, so that

$$\boldsymbol{\sigma}(x,y) = \boldsymbol{\sigma}_{ext} + \sum_{i=1}^{N} \boldsymbol{\sigma}_s(x,y). \tag{A.2}$$

The only non zero components of $\boldsymbol{\sigma}_s$ are

$$\sigma_{xz} = -\frac{\mu b}{2\pi}\frac{y}{x^2+y^2} \tag{A.3}$$

$$\sigma_{yz} = \frac{\mu b}{2\pi}\frac{x}{x^2+y^2}, \tag{A.4}$$

which can be differentiated with respect to x and y giving

$$\frac{\partial \sigma_{xz}}{\partial x} = -\frac{\partial \sigma_{yz}}{\partial y} = \frac{\mu b}{2\pi}\frac{2xy}{(x^2+y^2)^2} \tag{A.5}$$

$$\frac{\partial \sigma_{yz}}{\partial x} = \frac{\partial \sigma_{xz}}{\partial y} = \frac{\mu b}{2\pi}\frac{(y^2-x^2)}{(x^2+y^2)^2}. \tag{A.6}$$

Eq. A.2 can be simplified further to

$$\begin{aligned}\frac{\partial F}{\partial s} &= -2b\cos\theta\sin\theta\frac{\partial \sigma_{xz}}{\partial x} + b(\cos^2\theta - \sin^2\theta)\frac{\partial \sigma_{xz}}{\partial y} \\ &= -b\sin 2\theta\frac{\mu b}{2\pi}\frac{2xy}{(x^2+y^2)^2} + b\cos 2\theta\frac{\mu b}{2\pi}\frac{(y^2-x^2)}{(x^2+y^2)^2} \\ &= \frac{\mu b^2}{2\pi}\left[\frac{(y^2-x^2)\cos 2\theta - 2xy\sin 2\theta}{(x^2+y^2)^2}\right].\end{aligned} \tag{A.7}$$

In the DDP code, there is an additional factor of ± 1, depending on the sign of the dislocation. The stress components and the derivatives are plotted in Fig. A.1.

A.2 The edge dislocation

Similarly, for edge dislocations having same glide plane and glide direction, but with a Burgers vector $\boldsymbol{b} = (b_x, b_y, 0) = b(\cos\theta, \sin\theta, 0)$, one has that the magnitude of the glide component of the Peach-Koehler force is

$$F(x,y) = \hat{\boldsymbol{n}}\boldsymbol{\sigma}(x,y)\boldsymbol{b} = b\left[\frac{\sin 2\theta}{2}\Big(\sigma_{yy}(x,y) - \sigma_{xx}(x,y)\Big) + \cos 2\theta\sigma_{xy}(x,y)\right], \tag{A.8}$$

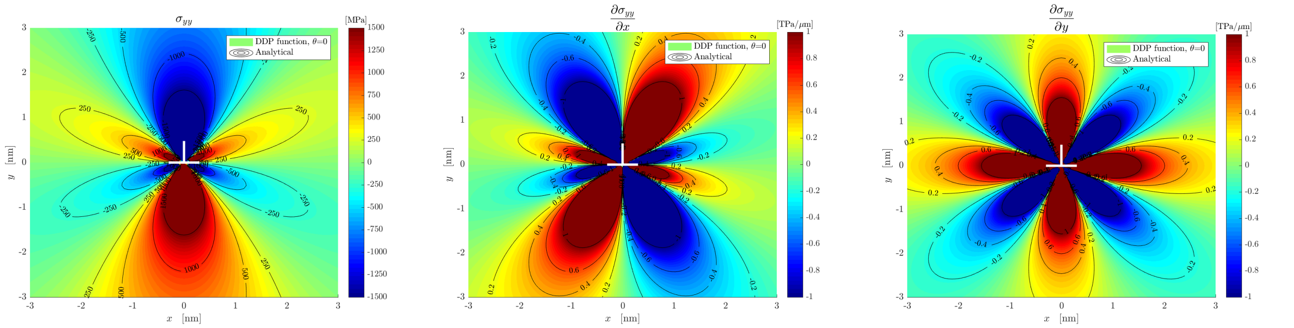

(a) (b) (c)

Figure A.2: Plots of the (a) σ_{yy} component, and of its partial derivatives with respect to x (b) and y (c), of an isolated edge dislocation at the origin. The colour plots were generated using the function included in the DDP code, setting $\theta = 0$.

and its directional derivative is

$$\begin{aligned}\frac{\partial F}{\partial s} = \; & b\cos\theta\left[\frac{\sin 2\theta}{2}\left(\frac{\partial\sigma_{yy}}{\partial x} - \frac{\partial\sigma_{xx}}{\partial x}\right) + \cos 2\theta\frac{\partial\sigma_{xy}}{\partial x}\right] \\ & + b\sin\theta\left[\frac{\sin 2\theta}{2}\left(\frac{\partial\sigma_{yy}}{\partial y} - \frac{\partial\sigma_{xx}}{\partial y}\right) + \cos 2\theta\frac{\partial\sigma_{xy}}{\partial y}\right].\end{aligned} \tag{A.9}$$

In this case, there are 6 derivatives of the stress components that need to be calculated to implement Eq. 6.

First, the stress tensor for an edge dislocation at the origin can be obtained using the Muskhelishvili's complex potentials [54]. Two complex-valued functions $\phi(z)$ and $\psi(z)$ exist such that

$$\sigma_{xx} + \sigma_{yy} = 2[\phi'(z) + \overline{\phi'(z)}] \tag{A.10}$$

$$\sigma_{yy} - \sigma_{xx} + 2i\sigma_{xy} = 2[\bar{z}\phi''(z) + \psi'(z)]. \tag{A.11}$$

To find the required stress components as a function of x and y, it is sufficient to calculate the real part of $\phi'(z)$ and the real and imaginary parts of $z\phi''(z)$ and $\psi'(z)$ with $z = x + iy$.

Considering an isolated dislocation at z_d, having a Burgers vector $\boldsymbol{b} = b_x + ib_y$. The orientation of the extra half plane can change, but as the magnitude of the Burgers vector is constant one has that $\boldsymbol{b} = be^{i\theta}$. The complex potentials are well known:

$$\phi = \frac{\mu b e^{i\theta}}{\pi(1-\kappa)i}\ln(z - z_d) \tag{A.12}$$

$$\psi = \frac{\mu b}{\pi(1-\kappa)}\left(ie^{-i\theta}\ln(z - z_d) - \frac{\overline{z_d}e^{i\theta}}{i(z - z_d)}\right). \tag{A.13}$$

κ is a constant that takes the value $(3 - 4\nu)$ in plane strain and $(3-\nu)/(1+\nu)$ in plane stress. In the implementation of DDP, only relative distances are important. Therefore, without loss of generality but with great simplification of the expressions, we choose $z_d = 0$.

The three stress components can be obtained combining Eq. A.10 and Eq. A.11 with the definitions in Eq. A.12 and Eq. A.13. The result is

$$\sigma_{xx} = 2\Re[\phi'] - (\Re[z\phi''] + \Re[\psi']) \tag{A.14}$$

$$\sigma_{yy} = 2\Re[\phi'] + (\Re[z\phi''] + \Re[\psi']) \tag{A.15}$$

$$\sigma_{xy} = \Im[z\phi''] + \Im[\psi'], \tag{A.16}$$

where

$$\Re[\phi'] = \frac{\mu b}{4\pi(1-\nu)} \frac{x\sin\theta - y\cos\theta}{x^2+y^2} \tag{A.17}$$

$$\Re[z\phi''] = \frac{\mu b}{4\pi(1-\nu)} \left[\frac{-x(x^2-3y^2)\sin\theta}{(x^2+y^2)^2} + \frac{y(3x^2-y^2)\cos\theta}{(x^2+y^2)^2} \right] \tag{A.18}$$

$$\Re[\psi'] = \frac{\mu b}{4\pi(1-\nu)} \frac{x\sin\theta + y\cos\theta}{x^2+y^2} \tag{A.19}$$

$$\Im[z\phi''] = \frac{\mu b}{4\pi(1-\nu)} \left[\frac{x(x^2-3y^2)\cos\theta}{(x^2+y^2)^2} + \frac{y(3x^2-y^2)\sin\theta}{(x^2+y^2)^2} \right] \tag{A.20}$$

$$\Im[\psi'] = \frac{\mu b}{4\pi(1-\nu)} \frac{x\cos\theta - y\sin\theta}{x^2+y^2} \tag{A.21}$$

The 6 derivatives in Eq. A.9 follow by differentiating Eqs. A.17-A.21. Both for the sake of brevity here, and for computational efficiency in the code, it is convenient to introduce the functions

$$f_1 = \frac{-x^2+y^2}{(x^2+y^2)^4} \tag{A.22}$$

$$f_2 = -\frac{2xy}{(x^2+y^2)^4} \tag{A.23}$$

$$f_3 = \frac{2xy(-3x^2+5y^2)}{(x^2+y^2)^6} \tag{A.24}$$

$$f_4 = -\frac{x^4-12x^2y^2+3y^4}{(x^2+y^2)^6} \tag{A.25}$$

$$f_5 = \frac{3x^4-12x^2y^2+y^2}{(x^2+y^2)^6} \tag{A.26}$$

$$f_6 = \frac{2xy(-5x^2+3y^2)}{(x^2+y^2)^6} \tag{A.27}$$

$$\tag{A.28}$$

so that the derivatives of the stress components can be defined as

$$\frac{\partial\sigma_{xx}}{\partial x} = \frac{\mu b[(f_1+f_4)\sin\theta - (3f_2+f_3)\cos\theta]}{4\pi(1-\nu)} \tag{A.29}$$

$$\frac{\partial\sigma_{xx}}{\partial y} = \frac{\mu b[(f_2+f_6)\sin\theta + (3f_1-f_5)\cos\theta]}{4\pi(1-\nu)} \tag{A.30}$$

$$\frac{\partial\sigma_{yy}}{\partial x} = \frac{\mu b[(3f_1-f_4)\sin\theta - (f_2-f_3)\cos\theta]}{4\pi(1-\nu)} \tag{A.31}$$

$$\frac{\partial\sigma_{yy}}{\partial y} = \frac{\mu b[(3f_2-f_6)\sin\theta + (f_1+f_5)\cos\theta]}{4\pi(1-\nu)} \tag{A.32}$$

$$\frac{\partial\sigma_{xy}}{\partial x} = \frac{\mu b[(f_3-f_2)\sin\theta + (f_1+f_4)\cos\theta]}{4\pi(1-\nu)} \tag{A.33}$$

$$\frac{\partial\sigma_{xy}}{\partial y} = \frac{\mu b[(f_1+f_5)\sin\theta + (f_2+f_6)\cos\theta]}{4\pi(1-\nu)}. \tag{A.34}$$

Fig. A.2 contains, as an example, the plots of σ_{yy} and of its partial derivatives. Both in Fig. A.2 and in Fig. A.1 the values given by the routine used in the DDP code were checked against the textbook expressions and their derivatives (these were included in the plots using black isocontours).

References

[1] B. Cox, "Some thoughts on the mechanisms of in-reactor corrosion of zirconium alloys," *Journal of Nuclear Materials*, vol. 336, no. 2-3, pp. 331–368, 2005.

[2] M. P. Puls, *The effect of hydrogen and hydrides on the integrity of zirconium alloy components: delayed hydride cracking*. Springer Science & Business Media, 2012.

[3] P. A. Olsson, A. R. Massih, J. Blomqvist, A. M. Alvarez Holston, and C. Bjerkén, "Ab initio thermodynamics of zirconium hydrides and deuterides," *Computational Materials Science*, vol. 86, pp. 211–222, 2014.

[4] H. Chung, R. Daum, J. Hiller, and M. Billone, "Characteristics of Hydride Precipitation and Reorientation in Spent-Fuel Cladding," *Zirconium in the Nuclear Industry: Thirteenth International Symposium*, pp. 561–561–22, 2002.

[5] J. S. Bradbrook, G. W. Lorimer, and N. Ridley, "The precipitation of zirconium hydride in zirconium and Zircaloy-2," *Journal of Nuclear Materials*, vol. 42, pp. 142–160, 1972.

[6] M. Grange, J. Besson, and E. Andrieu, "Anisotropic Behavior and Rupture of Hydrided ZIRCALOY- 4 Sheets," *Metallurgical and Materials Transactions A: Physical Metallurgy and Materials Science*, vol. 31, no. March, pp. 679–690, 2000.

[7] L. A. Simpson and C. D. Cann, "Fracture toughness of zirconium hydride and its influence on the crack resistance of zirconium alloys," *Journal of Nuclear Materials*, vol. 87, pp. 303–316, 1979.

[8] R. J. H. Wanhill, D. A. Ryder, and T. J. Davies, "Metallographic studies of fatigue in 20% cold-worked Zircaloy-2 containing zirconium hydride," *Journal of Nuclear Materials*, vol. 43, no. 2, pp. 75–85, 1972.

[9] S. Arsene, J. B. Bai, and P. Bompard, "Hydride embrittlement and irradiation effects on the hoop mechanical properties of pressurized water reactor (PWR) and boiling-water reactor (BWR) ZIRCALOY cladding tubes: Part I. Hydride embrittlement in stress-relieved, annealed, and recrystallized ZIRCALOYs at 20 °C and 300 °C," *Metallurgical and Materials Transactions A*, vol. 34, no. March, pp. 553–566, 2003.

[10] N. A. Veleva, S. Arsene, M.-c. Record, and J. L. U. C. Bechade, "Hydride Embrittlement and Irradiation Effects on the Hoop Mechanical Properties of Pressurized Water Reactor (PWR) and Boiling-Water Reactor (BWR) ZIRCALOY Cladding Tubes : Part II . Morphology of Hydrides Investigated at Different Magnifications and their interaction with the processes of plastic deformation," *Metallurgical and Materials Transactions A*, vol. 34, no. March, pp. 567–578, 2003.

[11] S. Arsene, J. Bai, and P. Bompard, "Hydride Embrittlement and Irradiation Effects on the Hoop Mechanical Properties of Pressurized Water Reactor (PWR) and Boiling-Water Reactor (BWR) ZIRCALOY Cladding Tubes : Part III . Part III. Mechanical behavior of hydride in stress-relieved annealed and recrystallized ZIRCALOYs at 20 °C and 300 °C," *Metallurgical and Materials Transactions A*, vol. 34, no. March, pp. 579–588, 2003.

[12] C. Q. Chen, S. X. Li, and K. Lu, "The deformation behaviors of gamma hydrides in titanium under cyclic straining," *Acta Materialia*, vol. 51, no. 4, pp. 931–942, 2003.

[13] C. Q. Chen, S. X. Li, and K. Lu, "Dislocation interaction with hydrides in titanium containing a low hydrogen concentration," *Philosophical Magazine*, vol. 84, no. November, pp. 29–43, 2004.

[14] C. Q. Chen, S. X. Li, H. Zheng, L. B. Wang, and K. Lu, "An investigation on structure , deformation and fracture of hydrides in titanium with a large range of hydrogen contents," *Acta Materialia*, vol. 52, no. 12, pp. 3697–3706, 2004.

[15] C. Q. Chen and S. X. Li, "Tensile and low-cycle fatigue behaviors of commercially pure titanium containing gamma hydrides," *Mater. Sci. Eng. A*, vol. 389, pp. 470–475, 2004.

[16] E. Conforto, I. Guillot, and X. Feaugas, "Solute hydrogen and hydride phase implications on the plasticity of zirconium and titanium alloys : a review and some recent advances," *Philosophical Transactions of the Royal Society A: Mathematical, Physical and Engineering Sciences*, vol. 375, no. 2098, 2017.

[17] H. E. Weekes, V. A. Vorontsov, I. P. Dolbnya, J. D. Plummer, F. Giuliani, and T. B. Britton, "In situ micropillar deformation of hydrides in Zircaloy-4," *Acta Materialia*, vol. 92, pp. 81–96, 2015.

[18] S. Wang, S. Kalácska, X. Maeder, J. Michler, F. Giuliani, and T. B. Britton, "The effect of δ-hydride on the micromechanical deformation of Zircaloy-4 studied by in situ high angular resolution electron backscatter diffraction," tech. rep., 2019.

[19] G. Carpenter, J. Watters, and R. Gilbert, "Dislocations generated by zirconium hydride precipitates in zirconium and some of its alloys," *Journal of Nuclear Materials*, vol. 48, pp. 267–276, 1973.

[20] G. J. C. Carpenter, "The dilatational misfit of zirconium hydrides precipitated in zirconium," *Journal of Nuclear Materials*, vol. 48, no. 3, pp. 264–266, 1973.

[21] H. Tummala, L. Capolungo, and C. N. Tome, "Quantifying the stress state in the vicinity of a δ-hydride in α-zirconium," *Journal of Nuclear Materials*, vol. 511, pp. 406–416, 2018.

[22] M. Patel, S. Waheed, M. R. Wenman, A. P. Sutton, and D. S. Balint, "Discrete Dislocation Plasticity Modeling of Hydrides in Zirconium under Thermal Cycling," *MRS Advances*, vol. 2, no. 55, pp. 3353–3358, 2017.

[23] E. Van der Giessen and A. Needleman, "Discrete dislocation plasticity: a simple planar model," *Modelling and Simulation in Materials Science and Engineering*, vol. 3, no. 5, pp. 689–735, 1995.

[24] A. A. Benzerga, Y. Bréchet, A. Needleman, and E. Van der Giessen, "Incorporating three-dimensional mechanisms into two-dimensional dislocation dynamics," *Modelling and Simulation in Materials Science and Engineering*, vol. 12, no. 59, pp. 159–196, 2004.

[25] J. Eshelby, F. Frank, and F. Nabarro, "The equilibrium of linear arrays of dislocations," *The London, Edinburgh, and Dublin Philosophical Magazine and Journal of Science*, vol. 42, no. 327, pp. 351–364, 1951.

[26] A. P. Sutton and R. W. Balluffi, *Interfaces in Crystalline Materials.* Oxford University Press, 2006.

[27] Y. Guo, T. B. Britton, and A. J. Wilkinson, "Slip band-grain boundary interactions in commercial-purity titanium," vol. 76, pp. 1–12, 2014.

[28] T. C. Lee, I. M. Robertson, and H. K. Birnbaum, "Prediction of slip transfer mechanisms across grain boundaries," *Scripta Metallurgica*, vol. 23, no. 8, pp. 799–803, 1989.

[29] J. P. Hirth and J. Lothe, *Theory of dislocations.* John Wiley & Sons, 1982.

[30] S. M. Hanlon, S. Persaud, F. Long, and M. Daymond, "Advanced Characterization of Hydrides in Zirconium Alloys," *Proceedings of the 18th International Conference on Environmental Degradation of Materials in Nuclear Power Systems - Water Reactors*, 2018.

[31] A. Cheadle and C. E. Ells, "The development of texture in zirconium alloy tubes," *Journal of Nuclear Materials*, vol. 23, pp. 199–268, 1967.

[32] M. N. Cinbiz, D. A. Koss, A. T. Motta, J. S. Park, and J. D. Almer, "In situ synchrotron X-ray diffraction study of hydrides in Zircaloy-4 during thermomechanical cycling," *Journal of Nuclear Materials*, vol. 487, pp. 247–259, 2017.

[33] J. Bair, M. Asle Zaeem, and M. Tonks, "A review on hydride precipitation in zirconium alloys," *Journal of Nuclear Materials*, vol. 466, pp. 12–20, 2015.

[34] G. Han, Y. Zhao, C. Zhou, D.-Y. Lin, X. Zhu, J. Zhang, S. Hu, and H. Song, "Phase-field modeling of stacking structure formation and transition of δ-hydride precipitates in zirconium," *Acta Materialia*, vol. 165, pp. 528–546, 2019.

[35] J. Gong, T. B. Britton, M. A. Cuddihy, F. P. E. Dunne, and A. J. Wilkinson, "⟨a⟩ Prismatic, ⟨a⟩ basal, and ⟨c+a⟩ slip strengths of commercially pure Zr by micro-cantilever tests," *Acta Materialia*, vol. 96, pp. 249–257, 2015.

[36] F. Onimus, L. Dupuy, and F. Mompiou, "Progress in Nuclear Energy In situ TEM observation of interactions between gliding dislocations and prismatic loops in Zr-ion irradiated zirconium alloys," *Progress in Nuclear Energy*, vol. 57, pp. 77–85, 2012.

[37] R. B. Adamson, "Cyclic deformation of neutron irradiated copper," *Phylosophical Magazine*, vol. 17, no. 148, pp. 681–693, 1968.

[38] F. Onimus, C. Prioul, and P. Pilvin, "A statistical TEM investigation of dislocation channeling mechanism in neutron irradiated zirconium alloys," *Journal of Nuclear Materials*, vol. 328, pp. 165–179, 2004.

[39] A. T. Motta, L. Capolungo, L.-Q. Chen, M. Nedim, M. R. Daymond, D. A. Koss, E. Lacroix, G. Pastore, A. Simon, M. R. Tonks, B. D. Wirth, and M. A. Zikry, "Hydrogen in zirconium alloys : A review," *Journal of Nuclear Materials*, vol. 518, pp. 440–460, 2019.

[40] H. Chan, S. G. Roberts, and J. Gong, "Micro-scale fracture experiments on zirconium hydrides and phase boundaries," *Journal of Nuclear Materials*, vol. 475, pp. 105–112, 2016.

[41] A. J. E. Foreman, "The bowing of a dislocation segment," *Phylosophical Magazine*, vol. 15, no. 137, pp. 1011–1021, 1967.

[42] S. S. Chakravarthy and W. A. Curtin, "New algorithms for discrete dislocation modeling of fracture," *Modelling and Simulation in Materials Science and Engineering*, no. 19, pp. 1–12, 2011.

[43] V. Ramachandran and R. E. Reed-Hill, "Dynamic strain aging and ductility minima in zirconium," *Metallurgical Transactions*, vol. 1, no. August, pp. 2105–2109, 1970.

[44] K. W. Lee, S. K. Kim, K. T. Kim, and S. I. Hong, "Ductility and strain rate sensitivity of Zircaloy-4 nuclear fuel claddings," *Journal of Nuclear Materials*, vol. 295, pp. 21–26, 2001.

[45] Z. Zheng, D. S. Balint, and F. P. E. Dunne, "Rate sensitivity in discrete dislocation plasticity in hexagonal close-packed crystals," *Acta Materialia*, vol. 107, pp. 17–26, 2016.

[46] J. Friedel, *Dislocations*. Pergamon, 1st ed., 1964.

[47] A. Benzerga, S. Hong, K. S. Kim, A. Needleman, and E. Van der Giessen, "Small is softer : an inverse size effect in a cast aluminium alloy," *Acta Materialia*, vol. 49, pp. 3071–3083, 2001.

[48] J. B. Bai, N. Ji, D. Gilbon, and J. L. Lebrun, "Microstructural study by XRD profile analysis and TEM observations on hydrided recrystallized Zircaloy-4," *Scripta Metallurgica et Materialia*, vol. 26, no. c, pp. 369–374, 1992.

[49] Z. Wang, U. Garbe, H. Li, Y. Wang, A. J. Studer, S. Guangai, R. P. Harrison, X. Liao, M. A. Vicente Alvarez, J. R. Santisteban, and C. Kong, "Microstructure and texture analysis of δ-hydride precipitation in Zircaloy-4 materials by electron microscopy and neutron diffraction," *Journal of Applied Crystallography*, vol. 47, no. 1, pp. 303–315, 2014.

[50] M. A. Vicente Alvarez, J. R. Santisteban, P. Vizcaíno, G. Ribárik, and T. Ungar, "Quantification of dislocations densities in zirconium hydride by X-ray line profile analysis," *Acta Materialia*, vol. 117, pp. 1–12, 2016.

[51] S. M. Hanlon, S. Y. Persaud, F. Long, A. Korinek, and M. R. Daymond, "A solution to FIB induced artefact hydrides in Zr alloys," *Journal of Nuclear Materials*, vol. 515, pp. 122–134, 2019.

[52] A. T. Barrow, A. Korinek, and M. R. Daymond, "Evaluating zirconium-zirconium hydride interfacial strains by nano-beam electron diffraction," *Journal of Nuclear Materials*, vol. 432, no. 1-3, pp. 366–370, 2013.

[53] J. Eshelby, "The determination of the elastic field of an ellipsoidal inclusion, and related problems," *Proceedings of the Royal Society of London A: Mathematical, Physical and Engineering Sciences*, vol. 241, no. 1226, pp. 376–396, 1957.

[54] N. Muskhelishvili, *Some Basic Problems in the Mathematical Theory of Elasticity*. JRM Radok (Noordhoff, Groningen), 1953.